Am J Physiol Cell Physiol 282: C606–C616, 2002.
First published October 31, 2001; 10.1152/ajpcell.00269.2001.

Cell prestress. I. Stiffness and prestress are closely associated in adherent contractile cells

NING WANG,[1] IVA MARIJA TOLIĆ-NØRRELYKKE,[1,3] JIANXIN CHEN,[1] SRBOLJUB M. MIJAILOVICH,[1] JAMES P. BUTLER,[1] JEFFREY J. FREDBERG,[1] AND DIMITRIJE STAMENOVIĆ[2]

[1]*Physiology Program, Department of Environmental Health, Harvard School of Public Health, Boston 02115;* [2]*Department of Biomedical Engineering, Boston University, Boston, Massachusetts 02215; and* [3]*Rugjer Bošković Institute, 10001 Zagreb, Croatia*

Received 14 June 2001; accepted in final form 24 October 2001

Wang, Ning, Iva Marija Tolić-Nørrelykke, Jianxin Chen, Srboljub M. Mijailovich, James P. Butler, Jeffrey J. Fredberg, and Dimitrije Stamenović. Cell prestress. I. Stiffness and prestress are closely associated in adherent contractile cells. *Am J Physiol Cell Physiol* 282: C606–C616, 2002. First published October 31, 2001; 10.1152/ajpcell.00269.2001.—The tensegrity hypothesis holds that the cytoskeleton is a structure whose shape is stabilized predominantly by the tensile stresses borne by filamentous structures. Accordingly, cell stiffness must increase in proportion with the level of the tensile stress, which is called the prestress. Here we have tested that prediction in adherent human airway smooth muscle (HASM) cells. Traction microscopy was used to measure the distribution of contractile stresses arising at the interface between each cell and its substrate; this distribution is called the traction field. Because the traction field must be balanced by tensile stresses within the cell body, the prestress could be computed. Cell stiffness (G) was measured by oscillatory magnetic twisting cytometry. As the contractile state of the cell was modulated with graded concentrations of relaxing or contracting agonists (isoproterenol or histamine, respectively), the mean prestress ($\bar{p}_t$) ranged from 350 to 1,900 Pa. Over that range, cell stiffness increased linearly with the prestress: G (Pa) = $0.18\bar{p}_t$ + 92. While this association does not necessarily preclude other interpretations, it is the hallmark of systems that secure shape stability mainly through the prestress. Regardless of mechanism, these data establish a strong association between stiffness of HASM cells and the level of tensile stress within the cytoskeleton.

tensegrity; mechanical stress; traction; cytoskeleton; actin microfilaments

CONTROVERSY SURROUNDS the tensegrity hypothesis (23, 28). As described below, some part of this controversy is perhaps attributable to insufficient precision in the use of associated terminology and some part to insufficient emphasis on underlying mechanisms on which tensegrity rests. The major part of the controversy, however, is surely attributable to the fact that tensegrity is a hypothesis that has been rich in opinions but poor in quantitative data. Few, if any, data have been available that could be used to put the hypothesis to a rigorous test.

The purpose of this series of companion papers is to amplify findings that have appeared recently in a brief report (55) and, in doing so, to bring to this controversy precision in the concepts, clarity about putative mechanisms, and new data that bear directly on the question itself. These data offer evidence that the tensegrity hypothesis, framed as it currently stands, captures certain central features of cell mechanical behavior but may be cast too narrowly.

We begin by addressing a somewhat broader question: by what central mechanism does the cytoskeleton of adherent cells develop mechanical stresses that oppose distortion of cell shape? The answer to this question is important in understanding many cellular functions, including spreading, migration, contraction, growth, and mechanotransduction (9, 13, 29). To answer this question, several models of cell mechanics have been advanced, including tensegrity (1, 11, 12, 15, 16, 22, 24, 25, 27, 28, 30, 39, 40, 42, 44–46, 48, 51, 56–59, 60). This universe of cell models divides into two distinct classes.

Continuum vs. discrete descriptions. The first distinct class comprises those models that start from the point of view of continuum mechanics. The continuum approach begins by consideration of an infinitesimally small element and the relationship of stress to strain in that element. The contributions of discrete stress-bearing elements, such as microfilaments, to the local stress-strain relationship at the microscale are replaced by an average within the element. The microscale behavior of these elemental components is described by differential equations governing mass conservation and force balances and is then integrated, subject to conditions prescribed at the cell boundary, to predict mechanical behavior at the macroscale (i.e., whole cell) level. This process leads to descriptions of stresses, strains, and displacements as continuous field variables throughout the cell body. These contin-

Address for reprint requests and other correspondence: N. Wang, Physiology Program, Harvard School of Public Health, 665 Huntington Ave., Boston, MA 02115 (E-mail: nwang@hsph.harvard.edu).

The costs of publication of this article were defrayed in part by the payment of page charges. The article must therefore be hereby marked "*advertisement*" in accordance with 18 U.S.C. Section 1734 solely to indicate this fact.

uum models can range from the simple to the complex, and they can have multiple subcompartments.

In contrast with continuum models, discrete models begin by consideration of discrete stress-bearing elements that are finite in size, perhaps even spanning an appreciable fraction of the cell body, as do microtubules (MTs) or stress fibers, for example. The cell is then presumed to comprise a large but finite number of these units, and they need not fill all space within the cell body (5, 51). As such, at this stage of the description, stresses and strains cannot be defined as continuous field variables. Instead, attention is turned to the forces and the displacements at each of the nodes where the discrete elements connect to one another (47). The behavior of the discrete elements is subjected to the constraints of a balance of forces at every node, compatibility conditions at every node (i.e., connected points must move together), and conditions prescribed at the cell boundary. This process yields the discrete nodal forces and nodal displacements throughout the cell body. At this stage, a coarse-graining average can be applied, and local stresses and strains can be computed as continuous field variables. The corresponding stress tensor is defined by the vector sum of forces borne by the discrete elements that transect a given surface, expressed per unit area of that surface. Like continuum models, discrete models can range from the simple to the complex, and they can have multiple subcompartments (51).

Stress-supported discrete structures. Among the family of discrete structures there is a special subclass called stress-supported structures (cf. Refs. 5, 8, 51). Within this subclass, discrete stress-bearing elements are postulated to carry preexisting tensile stresses even before an external load is applied; this initial state of tensile stress is called the prestress (cf. Ref. 8). When an external load is applied, the structural elements must move relative to one another, changing orientation and spacing until a new equilibrium configuration is attained (46). Changes of orientation and spacing of the discrete elements represent the central mechanism by which restoring forces arise in stress-supported structures (45, 46).

It follows that the bigger the initial tensile load carried by those discrete elements, the smaller will be the deformation that the structure must undergo before attaining a new equilibrium configuration. As such, as the prestress increases, the resistance to change of shape increases proportionally. This behavior is illustrated in familiar structures such as the simple pup tent, a rope hammock, a spider's web, or soap foam. These structures secure resistance to shape distortion from a distending prestress provided either by attachments to focal adhesions at the system boundary or, in the case of foams, by an inflating pressure (5, 48). Decrease the distending stress and the structure becomes floppy; take away the distending stress and the structure collapses. This idea leads to the primary characteristic of this class, namely, that resistance to shape distortion, as expressed by the system's stiffness, must increase in nearly direct proportion to the magnitude of the prestress (5, 45, 46).

In classic continuum theory, by contrast, all solids possess intrinsic stiffness because the infinitesimal element develops local stresses that oppose local shear even when the initial distending stress is zero. However, in stress-supported structures, stiffness and shape stability are maintained in the presence of prestress even when an intrinsic stiffness is lacking entirely.

Balancing the prestress. A secondary but nonetheless important question concerning stress-supported discrete structures is how the prestress is balanced. In this connection, a distinction has crept into the literature. In some systems the prestress is balanced in its entirety by connections to the system boundary, with the rope hammock and the spider's web being good examples. In other systems, though, most of the prestress is balanced by internal compression elements, sometimes called struts, that exist within the structure itself, with the posts of a pup tent and the inflating pressure of a foam being good examples. Turgor pressure in a plant leaf and the inflating pressure of a lung are still other examples (5, 46).

The main difference between these two types of stress-supported structures is that the force balance at each node includes only tensile forces in the former case but both compressive and tensile forces in the latter case. Despite this distinction, both share the same central mechanism by which they develop restoring forces that oppose changes of shape, namely, the prestress.

What is tensegrity? Unfortunately, the word "tensegrity" has come to mean different things to different investigators. Remarkably, these differences have never been articulated and, accordingly, have spawned at least a part of the controversy surrounding the hypothesis. In the structural mechanics literature, for example, a clear distinction is made between tensegrity structures and other stress-supported structures (51). Structures in which the prestress is balanced predominantly by internal struts are called tensegrity structures (21, 40, 47). We will refer to this as the structural form of the hypothesis, which then identifies tensegrity as a subclass of the more general family of stress-supported discrete structures.

An energetic form of the tensegrity hypothesis comes from mathematicians and is based on considerations of structural stability (cf. Ref. 10). According to this principle, all prestressed structures must assume an equilibrium configuration that minimizes the elastic energy stored in the structure. Insofar as this principle holds for all stress-supported structures, regardless of whether the prestress is balanced by internal compression elements, external objects, or a combination of the two, all pressure-supported structures are tensegrity structures.

In previous studies, Ingber and colleagues (cf. Refs. 27, 28) tended to use this latter notion of tensegrity, whereas Heidemann and colleagues (23, 28) used the former; this unstated difference in the usage of the

term tensegrity became the source of some contention and substantial confusion. The fundamental difference between the structural form and the energetic form of tensegrity is how prestress is balanced: the former requires that a substantial portion of the prestress is balanced by internal structural components, whereas the latter does not require them. Semantic and substantive issues aside, both are stress-supported structures.

Broadening the question. MTs have been put forward as candidates representing compression elements (27). Accordingly, the existence of internal cytoskeleton compressive elements has sometimes been taken as the sine qua non of the tensegrity hypothesis (23, 28). Nevertheless, it cannot be ruled out that the central mechanism by which stress-supported structures develop restoring forces, as described above, might still dominate even when the major part of the prestress is supported not by internal struts but, instead, by attachments to structures external to the cell such as the tractions that arise at the interface between the cell and the extracellular matrix on which the cell is spread.

This report deals with the primary characteristics of stress-supported structures, as described above, and the associated central mechanism. In particular, we have tested the a priori prediction for stress-supported structures, namely, that the stiffness of the cell must be directly proportional to the level of the cytoskeleton prestress (8). We have provided direct measurements of the cellular prestress and the relationship between changes of the prestress and changes in cell stiffness. A companion report (47) deals with the secondary characteristic of stress-supported structures, namely, the question of how that prestress is balanced. That article partitions the balancing compressive stresses between MTs and the extracellular structures, again using direct measurement methods. Both of these studies rest on a third article (7) that describes a new traction microscopy strategy that makes direct measurement of the prestress possible.

The first major result of this series of reports is that in contractile adherent cells, the cell stiffness and cell prestress are closely associated. This finding supports predictions derived a priori from the central mechanism described above. This finding does not necessarily disprove alternative models of cell deformability, which we have described below, or invalidate the continuum approach. The weight of the evidence does suggest, however, that the cell secures its stiffness mainly from the prestress. A second major finding, described in a companion article (47), is that in these cells, the MTs support an appreciable fraction of the prestress, but the fraction is relatively small.

METHODS AND MATERIALS

Experiments consisted of three major components: *1*) traction measurements with a polyacrylamide gel substrate, *2*) cell stiffness measurements with oscillatory magnetic cytometry, and *3*) measurements of F-actin distribution with confocal microscopy.

Cell culture. Human airway smooth muscle (HASM) cells were isolated from tracheal muscle of lung transplant donors (approved by the University of Pennsylvania Committee on Studies Involving Human Beings) using a method described previously (37). A monoclonal antibody that recognizes only smooth muscle-specific actin was used to identify the cells as smooth muscle cells. When cells reached *passage 2*, they were shipped to Boston for further experiments. Cells at *passage 3–6* were used for all experiments. These cells maintain smooth muscle cell morphology and physiological responsiveness to agonists until at least *passage 8* (37). After cells reached confluence in plastic dishes, they were serum deprived for 48 h before being trypsinized. The cells were then plated very sparsely (3,000–6,000 cells/dish) in serum-free medium on type I collagen-coated (0.2 mg/ml) polyacrylamide gel dishes for 4–6 h before experiments were conducted.

Polyacrylamide gel. We adapted the technique of polyacrylamide substrate described previously (14, 38). First, about five drops of 0.1 N NaOH were added to the 35-mm dish (glass bottom, uncoated, no. 0; MatTek, Ashland, MA) and air-dried. Next, 3-aminopropyltrimemethoxysilane (Sigma) was smeared onto dried dishes with a glass pipette just as if making a peanut butter sandwich. After 5 min, the dish was washed and soaked with distilled water. The dish was immersed for 30 min in 0.5% glutaraldehyde in PBS. Ten microliters of an acrylamide/bis-acrylamide mixture, containing 2% acrylamide and 0.1% or 0.25% bis concentrations, were added to the dish after being mixed with 0.2-μm-diameter fluorescent beads (1/125 volume of acrylamide mixture). The gel was covered with a small, circular piece of cover glass (no. 1, 12-mm diameter; Fisher) and turned upside down to let the microbeads move to the surface of the cover glass by gravity. After 45 min, the gel formed and the circular coverslip was carefully removed. Most microbeads moved to the free surface of the gel, as determined by microscopy. The gel was ~70 μm thick, as determined by confocal microscopy. To activate the free surface of the gel so that matrix proteins could be coated on it, 100 μl of 1 mM sulfosuccinimidyl-6-(4-azido-2-nitrophenylamino)hexanoate (Sulfo-SANPAH; Pierce) in 200 mM HEPES were pipetted onto the gel surface. The dish was exposed to ultraviolet light for 5 min, the Sulfo-SANPAH solution was removed, and the process was repeated once. The dish was washed with PBS twice. The gel was then coated with collagen type I and stored at 4°C.

Measurements of Young's modulus of the gel. The extracellular matrix-coated polyacrylamide substrate has superb optical quality and minimal thickness (~70 μm), which permit the observation of fluorescence at high magnifications. The gel also has nearly ideal elastic behavior and allows control of flexibility of the substrate by changing the relative concentration of acrylamide and bis-acrylamide (38). To calibrate the Young's modulus of the gel, the mixture of bis-acrylamide and acrylamide was placed in a 3-ml syringe. After the mixture was polymerized, the syringe was cut at ~2 cm in length. One piece of plastic (made from the bottom of 1 well of the 96-well dish) with one hook on one end was glued onto one end of the gel. The gel strip was then carefully pulled from the syringe, and the other end of the gel was glued to another piece of plastic. The gel strip was connected to the force-displacement apparatus (35) by using the two hooks, and the force-displacement relationship was measured. The resultant forces were obtained when step functions of uniaxial tensile strains were applied at 1, 2, 4, 6, 8, and 10%. The stress was calculated as force per unit cross-sectional area of the gel strip. The stress-strain relationship was found to be linear. The Young's modulus was calculated as the slope of this relationship. The Young's modulus of 0.1% bis and 2%

acrylamide gel was determined to be 870 Pa (range: 863–1,000 Pa), and that of 0.25% bis and 2% acrylamide was 1,300 Pa (range: 920–1,630 Pa). The modulus of the gel varied <10% when temperature was varied from 25 to 37°C or when the gel was treated with agents such as histamine, colchicine, or trypsin.

Measurements of traction, contractile force, prestress, and contractile moment. To determine the displacement field of the gel as the adhering cell contracted or relaxed, we used the method of Butler et al. (7). In brief, images of the same region of the gel were taken at different times. Images were then divided into a number of small window areas. The displacement field between a pair of images was obtained by identifying the coordinates of the peak of the cross-correlation function of each pair of window areas. The two-dimensional fast Fourier transform algorithm in MATLAB was used to calculate the correlation functions. The traction field was calculated from the displacement field, implementing the solution described by Butler et al. (7). This calculation was based on the Boussinesq solution for the displacement field on the surface of a semi-infinite solid when the distribution of surface traction was known. Writing the displacements as a convolution of tractions and the kernel that mapped tractions to displacements and then taking the Fourier transform of this relation yielded the solution for the traction field on the surface, when the surface displacement field and the gel elastic properties were known. The traction field was obtained by repetitive calculations from the displacement field using constrained Fourier transform traction cytometry. The boundary conditions were as follows: *1*) zero traction outside the cell-gel interfacial area, and *2*) the displacement field within the cell-gel interface matched the experimentally observed displacements within the cell boundary. The Poisson's ratio of the gel was assumed to be 0.48 (values obtained for traction increased by <2% if the Poisson's ratio was assumed to be 0.3). The traction field was used to obtain the prestress, defined as the net tensile force transmitted by the actin cytoskeleton across a cross-sectional area of the cell per unit area.

The mean prestress was obtained by considering a force balance of a section of the cell (Fig. 1)

$$\bar{p}_t A'' = \bar{t} A' \qquad (1)$$

where $\bar{p}_t$ is the mean prestress, $\bar{t}$ is the mean traction, A' is the interfacial area, and A'' is the cross-sectional area of the cell section; $\bar{t} = (1/A')\int_A \mathbf{t}\cdot\mathbf{n}dA$, where $\mathbf{t}$ is the traction vector field and $\mathbf{n}$ is the unit normal vector to the cross-sectional area. As noted earlier, the stress is defined as the force per unit cross-sectional area of cell; the volume fraction of stress-bearing elements within the cell, while of some interest and possibly changing during the course of the experiments due to actin polymerization or depolymerization, was not needed for this calculation. We have addressed this point in DISCUSSION.

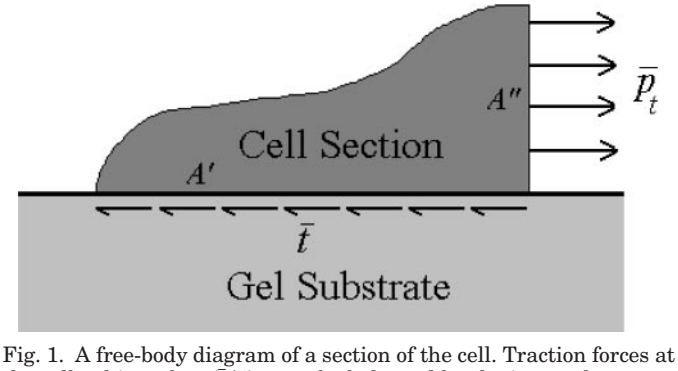

Fig. 1. A free-body diagram of a section of the cell. Traction forces at the cell-gel interface ($\bar{t}A'$) must be balanced by the internal stresses in the cell body ($\bar{p}_t A''$). This $\bar{p}_t A'' = \bar{t}A'$ where $\bar{p}_t$ is the mean prestress, $\bar{t}$ is the mean traction, A' is the interfacial area, and A'' is the cross-sectional area of the cell section.

First, the orientation of the principal tractions was calculated (7). Next, the cell was intersected by imaginary planes perpendicular to the surface of the gel and perpendicular to the principle axis of traction. The distance between the successive planes was the same (~2.7 μm) as between the points of the lattice on which the forces were calculated. The maximum cumulative contractile force was obtained when the product of the traction and the interfacial area of a cell section $\bar{t}A'$ reached maximum, usually over the nucleus. The cross-sectional area was calculated as the area of a segment of a circle by using the height of the cell as the height of the segment and the length of the line intersecting the projected area of the cell as the length of the secant of a circle. The height at each section of the cell was calculated by assuming that the height of the cell at the nucleus is 6 μm (confocal microscopy images showed that it was ~6 μm) and that it decreases linearly toward the edges of the cell to 0.5 μm. The projected area was measured by drawing a boundary of the cell in the phase-contrast images. The average $\bar{p}_t$ was calculated for all the sections.

Finally, the net contractile moment was calculated as described by Butler et al. (7). The net contractile moment is a scalar measure of the cell's contractile "strength" and is useful because it is directly derived from the traction field with no additional geometrical information. The formal definition is given by Butler et al. (7), but the contractile moment can be thought of loosely as an equivalent force generator comprising only two imaginary point forces (F) that are equal, opposite, and separated by a distance (d). This equivalent force generator "pinches" the elastic substrate to the same extent as does the cell. The contractile moment (M) is simply the product Fd (see Fig. 4*B*).

If the geometry of the adherent cell does not change appreciably during the contractile event, it follows on dimensional grounds that the prestress must be proportional to the contractile moment.

Protocols. After the control images of the cell and fluorescent microbead markers were recorded, increasing concentrations of histamine (0.1, 1, and 10 μM) or isoproterenol (0.01, 0.1, 1, and 10 μM) were added sequentially every 3 min, and fluorescent images were recorded every 40 s. After the treatments were completed, the cell was trypsinized and the cell-free bead positions were recorded as a reference point for bead displacement.

Oscillatory magnetic twisting cytometry. This technique is an extension of the previous magnetic twisting cytometry technique that used step twists (52–54). According to the method of Maksym et al. (33), a sinusoidally varying vertical magnetic field (0.1 Hz, 8 Pa, peak to peak) was applied to ferromagnetic beads attached to the integrin receptors on the cell apical surface after the beads had been magnetized at a 45° angle from the horizontal direction (33). Resulting bead rotation was determined by measuring the oscillating remnant magnetic field produced by the beads. The dynamic modulus was defined in the frequency domain as a complex ratio of the twisting specific torque and the corresponding angular rotation. The in-phase component of modulus was the storage modulus (elasticity or stiffness). This method greatly reduces the effects of heterogeneous bead rotations. RGD-coated ferromagnetic microbeads (4.5-μm diameter; average: 2 beads/cell) were added to the cells plated for 4–6 h on

type I collagen-coated rigid dishes (96-well plate, Immunon II; Dynetec) for 20 min. Unbound beads were washed away with serum-free medium, and then the magnetic twisting was performed.

Confocal microscopy. To determine the spatial distribution of actin microfilaments in HASM cells, we plated the cells on type I collagen-coated cover glasses for 4–6 h in serum-deprived medium and fixed them with 4% formaldehyde. The cytoskeletal buffer was then added to permeabilize the membrane. The rhodamine-phalloidin was added at 200 nM, and the cells were visualized with a laser confocal microscope (TCS NT; Leica).

Data analysis. Statistically significant differences between groups of data were assessed by two-tailed paired *t*-tests. Two-tailed *t*-tests for correlation coefficients also were performed. In both tests, differences with $P < 0.05$ were considered significant.

RESULTS

The cells cultured on a flexible polyacrylamide gel were stimulated with graded doses of a contractile agonist (histamine) or a relaxing agonist (isoproterenol). After cells were stimulated with histamine (Fig. 2), the bead displacement field was determined. When the cells were contracted with histamine, the displacement vectors were directed toward the nucleus, the largest displacements were observed at the two ends of the cell, and there was little displacement underneath the nucleus (Fig. 3). Similarly, the greatest traction was at the two ends of the cell, and there was little traction underneath the nucleus (Fig. 4*A*). The root mean square traction averaged over the entire cell projected area increased progressively with increasing doses of histamine (Fig. 5*A*). In contrast, the average traction decreased progressively with increasing doses of isoproterenol (Fig. 5*B*), indicating that the cell basal tone decreased in response to isoproterenol.

The cell stiffness (G) measured by the oscillatory magnetic twisting cytometry also increased in response to increasing doses of histamine and decreased in response to increasing doses of isoproterenol (Fig. 6). These changes are consistent with previous findings (26, 32, 36).

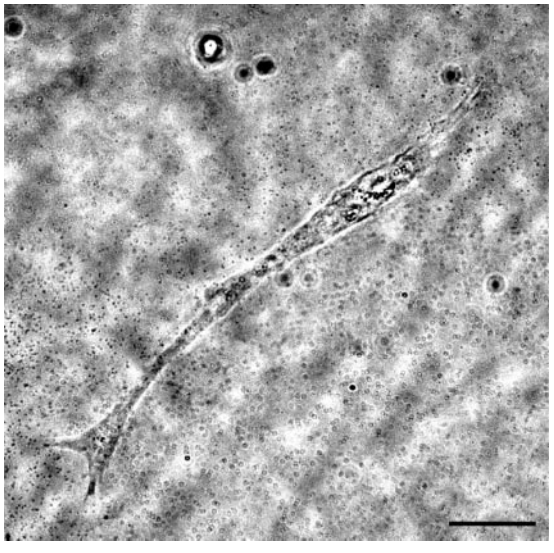

Fig. 2. A phase image of a human smooth muscle cell cultured on the polyacrylamide gel coated with collagen type I, 3 min after treatment with 10 μM histamine. The average projected area of all cells (n = 17) was 2,628 ± 191 μm^2. Data are means ± SE. Bar, 20 μm.

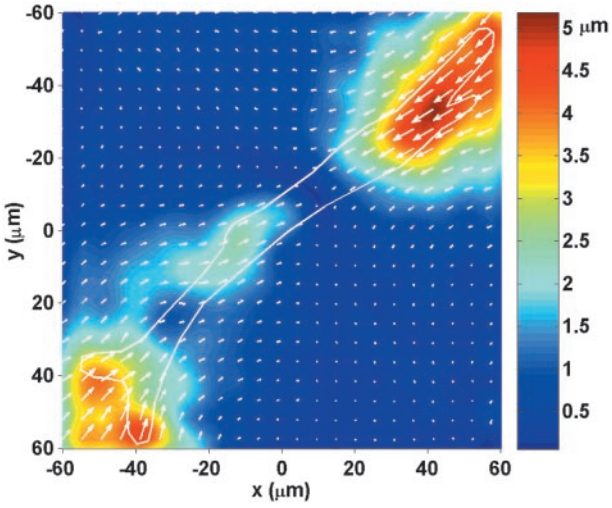

Fig. 3. The displacement field computed from the 2 fluorescent images of the 0.2-μm-diameter microbeads in the gel (the condition at 3 min after histamine relative to the cell-free condition). Arrows show the direction and magnitude of the displacement field of the gel under the cell. Colors show the absolute magnitude of the displacements in μm.

From the traction field, we computed three metrics of the prestress. The first was derived from a force balance struck at a section of the cell perpendicular to its long axis (Fig. 1), with the stress given as the net force normalized by the cell cross-sectional area, estimated as described in METHODS AND MATERIALS. The prestress increased with increasing doses of histamine and decreased with increasing doses of isoproterenol. The magnitude of the prestress was much higher than that of the average traction because of a much smaller cell cross-sectional area compared with the interfacial contact area (*Eq. 1*) (Fig. 7, *A* and *B*).

As the contractile state of the cell was modulated with graded concentrations of relaxing or contracting agonists (isoproterenol or histamine, respectively), the mean prestress ($\bar{p}_t$) ranged from 350 to 1,900 Pa. Over that range, cell stiffness increased linearly with the prestress: G (Pa) = $0.18\bar{p}_t + 92.43$ ($r^2 = 0.966$, $P < 0.01$) (Fig. 8, *top inset*).

A drawback of this particular metric, however, is that errors in estimation of the cell cross-sectional area contribute directly to errors in the estimate of the prestress. The second method used was a variant on the first in which we found the location along the cell body that yielded the largest net traction force (f) and then used that force as an index of the prestress but did not normalize for the cell cross-sectional area, thereby avoiding any systematic errors associated with the area measurement. This method also yielded a linear relationship: G (Pa) = $3.77f - 2.44$ ($r^2 = 0.984$, $P < 0.01$) (Fig. 8, *bottom inset*). The third method used was to obtain the net contractile moment M, as described in METHODS AND MATERIALS and Butler et al. (7), as an index

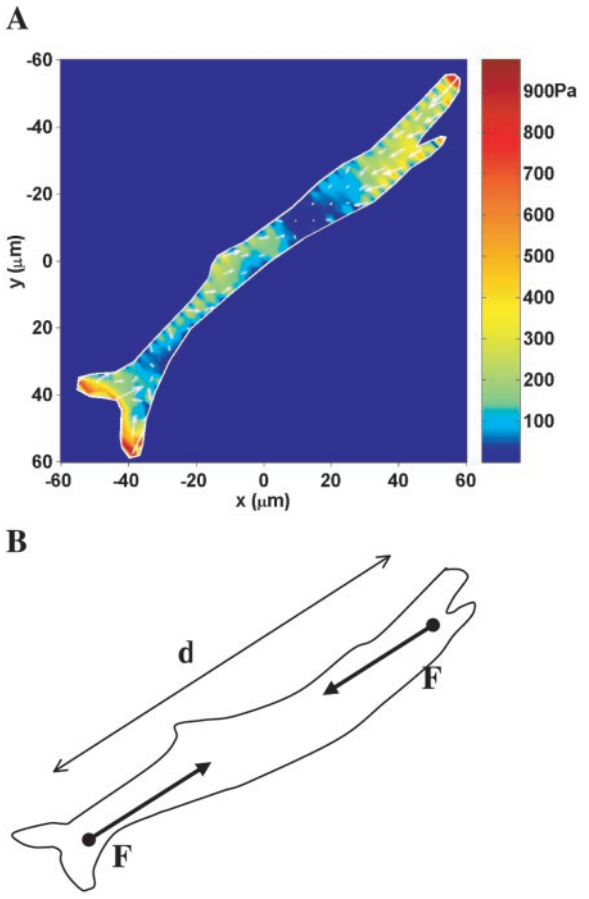

Fig. 4. *A*: the traction field computed from the displacement field shown in Fig. 3. Arrows show the direction and relative magnitude of the tractions. Colors show the magnitude of the traction vectors in Pa. Young's modulus of the gel was 1,300 Pa. *B*: illustration of how the net contractile moment was calculated: the traction field was replaced with 2 equal and opposite point forces (F) separated by a distance (d). The net contractile moment was the dipole strength (Fd).

of the prestress. This relationship also was found to be linear: G (Pa) = $39.96M + 4.51$ ($r^2 = 0.985$, $P < 0.01$) (Fig. 8).

Three-dimensional confocal microscopy showed that actin microfilaments were distributed throughout the depth of the cytoplasm, except for the nucleus (Fig. 9).

DISCUSSION

The primary finding of this study is a strong association between cell stiffness and the level of tensile stress within the cytoskeleton. Both increased in a coordinated dose-dependent fashion with increasing concentrations of histamine and decreased with increasing concentrations of isoproterenol. We will begin by addressing limitations of the methods that we have employed and then discuss the central finding and underlying mechanisms.

Oscillatory magnetic twisting cytometry. We used oscillatory magnetic twisting to obtain a quantitative index of cell stiffness and its changes. With this method, magnetic fields are used to apply an oscillatory mechanical torque to magnetic beads that are coupled to the actin cytoskeleton network through cytoplasmic tails of integrins (6, 33, 52). Changes of cell stiffness measured previously with conventional step twists have been shown to provide a reliable qualitative index of the contractile status of HASM cells (26). For example, this approach has become a standard tool to elaborate signal transduction pathways in these cells (32) and to link differences in β_2-adrenergic receptor genotype to differences in cell mechanical function (36).

Maksym et al. (33) showed that the step-twist protocol substantially underestimates cell stiffness, however, and identified two factors that contribute to that underestimation. The first concerns the use of an "apparent" stiffness (52–54). The apparent stiffness, as used previously, is derived from a step-twist measure-

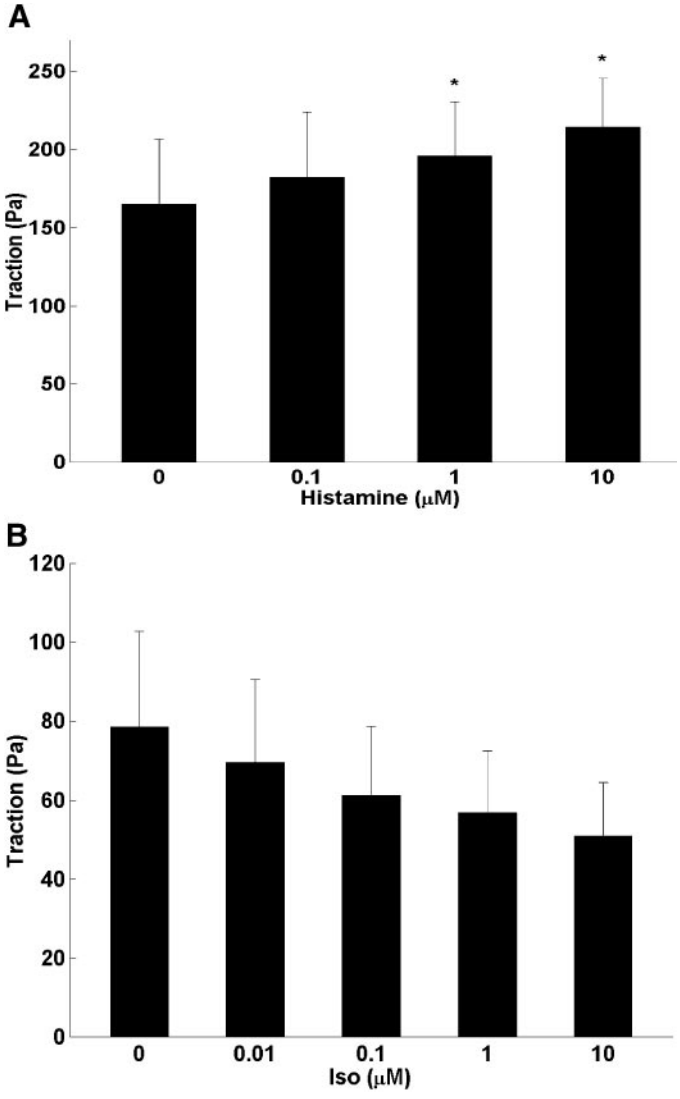

Fig. 5. Traction increased with contractile agonists and decreased with relaxing agonists. Calculated traction (root mean square) of human airway smooth muscle (HASM) cells is shown as a function of contractile or relaxing agonists after treatment with histamine (*A*) and after treatment with isoproterenol (Iso; *B*). Data are means ± SE; $n = 13$ cells for *A* and 4 cells for *B*. *$P < 0.05$.

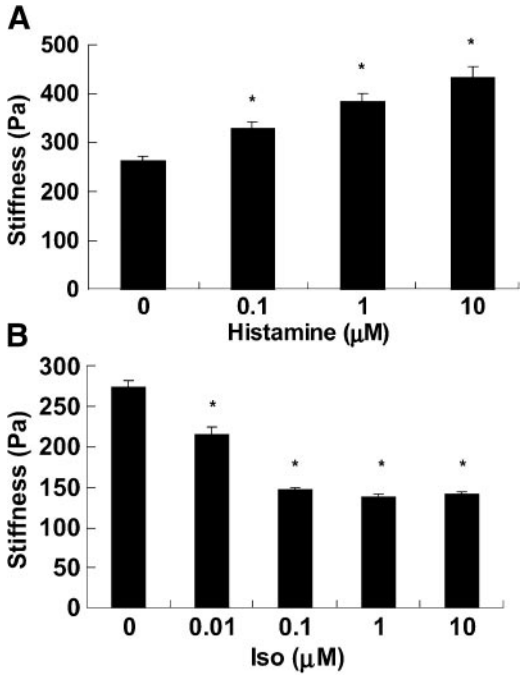

Fig. 6. Stiffness increased with contractile agonists and decreased with relaxing agonists. Stiffness of HASM cells is shown in response to different doses of histamine (*A*) or isoproterenol (*B*). Cells were plated on rigid dishes coated with collagen type I. Ferromagnetic beads were added for 20 min, sinusoidal oscillatory twisting fields (0.1 Hz, 8 Pa) were applied, and the elastic stiffness was measured. In *A*, $P < 0.005$ for 0.1, 1, and 10 μM histamine treatments compared with baseline, respectively; in *B*, $P < 0.004$ for 0.01, 0.1, 1, and 10 μM isoproterenol treatments compared with baseline, respectively. $P < 0.05$ between all successive treatments except between 1 and 10 μM isoproterenol. Data are means ± SE; $n = 8$ wells for *A* and 8 wells for *B*. *$P < 0.05$.

ment; this apparent stiffness does not correspond solely to the cell's elastic properties because it includes both elastic and frictional responses. The second factor accounting for the underestimation is the contribution to the magnetic signal arising from beads that rotate easily because they are only loosely bound to cell surface or form a part of a bead chain (18, 33). Maksym et al. (33) showed that with two changes in the experimental method, the contribution of both of these factors could be reduced dramatically. In addition, use of an oscillatory twisting field, as opposed to a step twist, allows mechanical responses to be separated into distinct elastic (real) and frictional (imaginary) components and allows their dependence on frequency of oscillation to be measured. Use of an initial magnetization angle of 45°, as opposed to 90°, markedly attenuated the contribution of loosely bound beads and bead chains. Together, these changes lead to quantitative estimates of cell stiffness that are larger by about one order of magnitude compared with the apparent stiffness derived from step twists.

A model of cell deformation must be invoked to relate raw data to estimates of the cell stiffness, regardless of whether the raw data are obtained from magnetic twisting as described here, micropipette aspiration, cell poking, atomic force microscopy, or tracking microrheology (25, 41, 60, 61). Using a simple homogeneous finite element model of cell deformation induced by twisting a bead that is partially embedded, we have estimated the shear stiffness at baseline to be ~250 Pa (Fig. 6*A*), which compares with the range reported for endothelial cells of ~100–130 Pa (43, 50) and for chondrocytes of ~220 Pa (30) (converted from Young's modulus, assuming material isotropy and incompressibility). While absolute values of the shear modulus are of interest, the main concern in this report is a reliable index of its relative changes. Available evidence supports the idea that oscillatory magnetic twisting cytometry as developed by Maksym et al. (33) and as used here provides an adequate index.

Traction microscopy. We used traction microscopy to measure the traction field that the cell applied to its substrate and to compute indices of the cell prestress

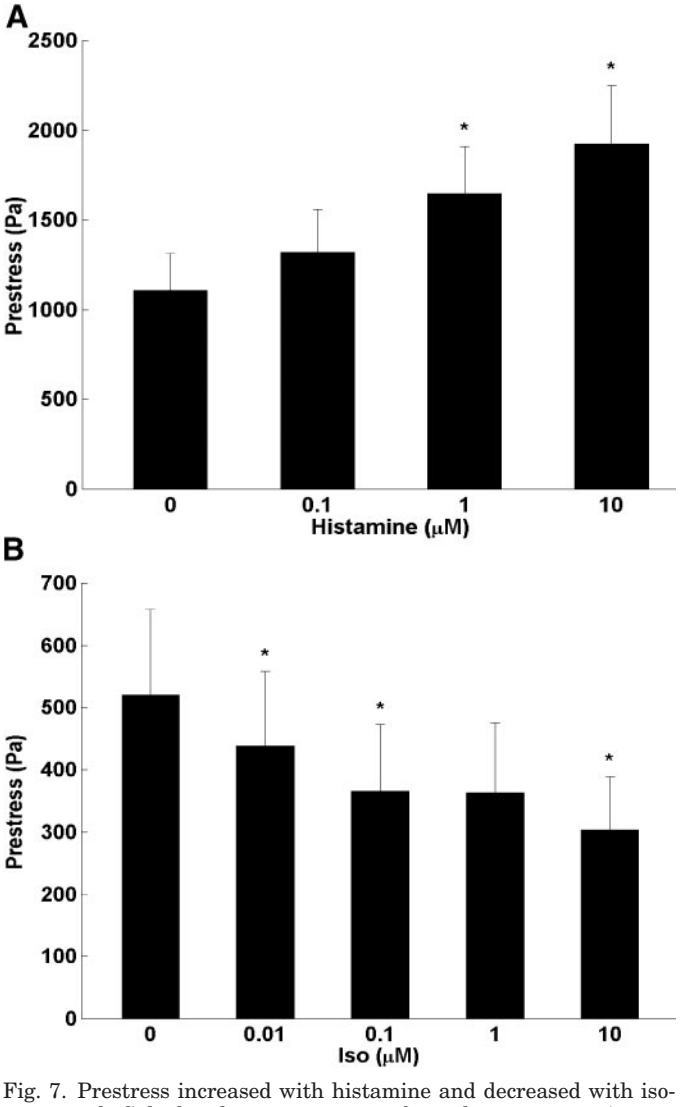

Fig. 7. Prestress increased with histamine and decreased with isoproterenol. Calculated mean prestress from the mean traction according to *Eq. 1* is shown after treatment with histamine (*A*; $P < 0.02$ between 1 and 10 μM histamine treatment and baseline) and after treatment with isoproterenol (*B*; $P < 0.04$ between 0.01, 0.1, and 10 μM Iso treatments and baseline). Data are means ± SE; $n = 13$ cells for *A* and 4 cells for *B*. *$P < 0.05$.

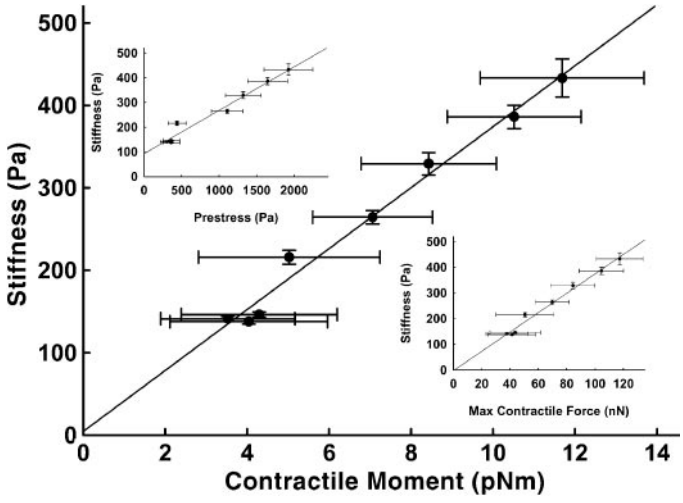

Fig. 8. Stiffness varied proportionally with contractile moments, prestress, and contractile force. The relationship between the stiffness and the net contractile moment is shown. *Top inset*: relationship between the stiffness and the prestress obtained from the data in Figs. 6 and 7. *Bottom inset*: relationship between stiffness (from Fig. 6) and the maximum contractile force. Data are means ± SE; $n = 13$ cells for contractile force and contractile moment measurements.

from the measured traction field (7). The issues of concern with this technique surround the spatial resolution of the computed traction field, accuracy in tracking the fiducial markers within the elastic substrate, and estimation of certain geometrical factors that contribute to the estimate of the prestress and the associated choice of the prestress metric.

The spatial resolution of the traction field is the same as that of the displacement field (7). The spatial resolution of the fluorescent microbead images is ~0.2 μm, and that of the displacement field images is ~0.4 μm. In comparison, a recent report describing use of a different algorithm reliably retrieved local contact forces with a resolution of >3 μm (3). In general, there could be artifacts associated with density, distribution, and depth of the embedded fluorescent beads, the focus plane relative to the beads, and the presence of nearby cells. These artifacts were minimized with the application of appropriate procedures described in METHODS AND MATERIALS and in Ref. 7. We used a cross-correlation approach that allows semiautomated estimates of the displacement field without the necessity to identify individual beads between images, and thus the potential artifacts associated with identifying individual beads were reduced (7). In addition, the measured traction field is a measure of the contractile forces only in the *x-y* plane (Fig. 1), and thus components of the contractile force out of the plane, if any, were not measured. However, the displacements of out-of-plane beads were very small (~0.2 μm).

There were two likely sources of variability in the traction measurements. The stiffness of HASM cells is known to vary from well to well and from donor to donor and can vary appreciably between adjacent cells cultured on the same day from the same donor in the same well (19). It might be expected, therefore, that tractions exhibit a comparable degree of variability between cells. A second source of variability derives from differences in the Young's modulus of gel substrates made on different days, which was appreciable (see METHODS AND MATERIALS).

Cell stiffness vs. prestress. From the traction field, we computed three metrics of the prestress. Although there were slight differences among these methods, each showed that the measured changes in cell stiffness varied in a coordinate fashion with induced changes in the level of tensile stress within the cytoskeleton (Fig. 8). The first method displayed a non-zero intercept, whereas the other two showed close-to-zero intercepts (Fig. 8). Because the first metric utilized geometric information, whereas the latter two did not, we suspect that part of the non-zero intercept may reflect a bias in the measurement of the cell cross-sectional area. Therefore, the data indicate a strong linear association between cell stiffness and cell prestress independent of the details of cell geometry.

There is one slight inaccuracy in the above argument that we now take into account. The metrics of the prestress, as described above, represent only that portion of the contractile stress that is balanced by the traction at the interface between the cell and its substrate. In other words, the traction is the net force per unit area transmitted from the cell to the substrate. Intracellular compression-supporting structures such as MTs also may contribute to the stress balance. However, in a companion study (47), we showed that

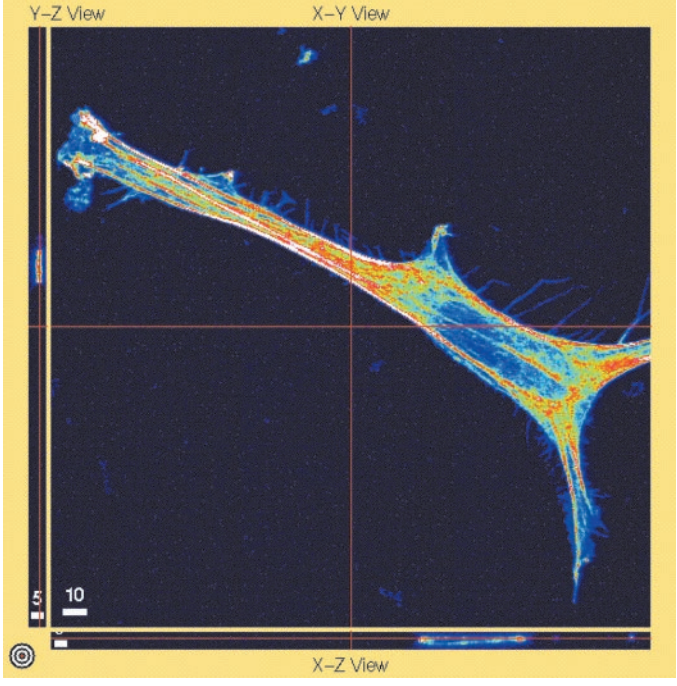

Fig. 9. Actin microfilaments were distributed throughout the cytoplasm. A representative image of filamentous actin in a spread HASM cell is shown. The cell was stained with rhodamine-phalloidin and visualized in the *x-y* plane, *x-z* plane, and *y-z* plane with a laser confocal microscope (scale bars: 10 μm in *x-y* view, 5 μm in *x-z* and *y-z* views). Note that the actin microfilaments are dense (yellow-reddish color) in the depth of the cytoplasm.

MTs contributed only slightly (14% on average) to the force balance. This implies that the slope of the relationship of cell stiffness vs. prestress in Fig. 8 may be overestimated to the same extent.

What might be the source of the prestress in an adherent cell? Besides the active contractile forces generated by the actomyosin apparatus, there could be other passive and active forces such as adhesion forces between the extracellular matrix and the focal adhesions, cell-cell contact forces if there are cell-cell contacts, transmembrane pressure differences, and possibly other pressure-induced (e.g., transpulmonary pressure or systemic blood pressure) and/or shear flow-induced deformation in vivo that contribute to the presence of prestress.

Potential mechanisms for a close association between stiffness and prestress. We considered three mechanisms that might account for the observed association between the prestress and the cell stiffness. The first is polymerization of the actin lattice. It is known that contractile agonists, in addition to causing smooth muscle cells to generate force by the actomyosin mechanism, also result in actin polymerization (34, 49). Thus the increase in both the prestress and the cell stiffness could be the result of nothing more than actin polymerization induced by contractile activation. However, a recent study in HASM cells argues against this interpretation. Blocking actomyosin force generation at the level of myosin in a variety of ways (2,3-butanedione monoxime to inhibit myosin ATPase activity, ML-7 to inhibit myosin light chain phosphorylation, or W-7 to antagonize calmodulin) ablates changes of cell stiffness observed in response to contractile activation but does not inhibit actin polymerization (2). Therefore, the increases of cell stiffness and traction reported with contractile activation, as studied here, cannot be attributable to polymerization of F actin.

Although we do not exclude an important role for actin polymerization, these data suggest that the myosin motor may dominate the mechanical response, as might be expected in a muscle cell. While the role of actin polymerization alone or together with possible myosin recruitments to these newly polymerized microfilaments remains uncertain, we favor the interpretation that the mechanical changes reflected in the results reported here are attributable mainly to activation of the contractile machinery within the cell.

This leads to the second potential mechanism, namely, that the changes of stiffness and prestress are both direct effects of myosin cross-bridge recruitment. It is known from studies of isolated muscle strips in longitudinal extension that muscle force and muscle stiffness both depend directly on the number of the attached cross bridges and, therefore, display a close association with one another (20). If so, then the changes shown in Figs. 6 and 7 could reflect nothing more than the direct effects of changing numbers of attached cross bridges within the cytoskeleton lattice; as the number of attached cross bridges increases in response to contractile agonists, both traction and cell stiffness would increase in parallel. Other data argue against this interpretation, however. Muscle stiffness measured in the longitudinal extension shows a characteristic change in that as the frequency of the length oscillation is increased, the stiffness increases and then reaches a plateau as the frequency of oscillation approaches and then exceeds bridge cycling rates (31). In contrast, the cell stiffness measured with oscillatory magnetic twisting does not exhibit frequency dependence that is characteristic of bridge cycling kinetics. Instead, it exhibits a weak power law dependence throughout a wide range of frequencies (17). This finding is not consistent with a direct effect of myosin cross bridges and leads to the third potential mechanism, which is an indirect effect of myosin motors as described below.

Tensegrity. The central hypothesis that we set out to test is that the cell behaves as a stress-supported discrete structure. As such, activation of the myosin-based contractile machinery of the cell would be predicted to increase the tensile force in actin filaments, which, in turn, would stiffen the lattice by the mechanism described in the Introduction. This hypothesis leads to the testable prediction that in stress-supported structures, there must exist a close association between cell stiffness and the cell prestress. Although we do not rule out alternative explanations, the data presented here are consistent with this a priori prediction and suggest that changes in cell stiffness in these cells were accounted for by induced changes in the prestress in the actin lattice that are secondary to changes in actomyosin force generation.

Common stress-supported models of cell deformability include the cortical membrane model (15, 16, 24, 59), the cable nets model (44), and the tensegrity model (10, 27, 46). The cortical membrane model and the cable nets model depict the cell as a two-dimensional cortical membrane or two- and three-dimensional tensile nets, whereas the tensegrity model emphasizes the importance of intracellular compression-supporting structures. Our results alone cannot discriminate between these models. However, our data showing that actin microfilaments are distributed throughout the cytoplasm (Fig. 9) are not consistent with the cortical membrane model. Other cytoskeleton structures (e.g., the spectrin lattice) in the cell cortex may contribute to the stiffness of the cell at zero prestress, but on the basis of the data in Fig. 8, this contribution to the cell stiffness would appear to be small.

In a companion paper (47), we show that in physiological conditions, compression of MTs balances 14% of the prestress, with the rest being balanced by stresses in the cell substrate to which the cell is adherent. If MT depolymerization by colchicine were incomplete, then the estimated fraction of the prestress balanced by compression in MTs might be somewhat higher but would still represent only a small fraction of that supported by the substrate. This finding does not preclude the possibility that, in other conditions and/or in other cell types, the majority of the prestress might be balanced by internal compression members. For instance, it has been shown that MTs balance >50% of

the contractile forces in fibroblasts cultured in collagen lattices (4). Nonetheless, data reported here suggest that the majority of the prestress in these spread HASM cells was not balanced by internal struts.

In the end, do adherent cells conform to the tensegrity hypothesis? The data in this report show that the answer would be a tentative "yes" according to the structural form of the tensegrity hypothesis; a small but statistically significant portion of the prestress was borne by internal struts. Furthermore, in certain cells, MTs contributed to >50% of the prestress (4), and clear determination of their role awaits future studies examining the effects of varying extracellular matrix compliance and cell-spreading areas over a wide range. The answer is a definite "yes" according to the energetic form of the tensegrity hypothesis. Nevertheless, the data are consistent with the hypothesis that the cell prestress is indeed a stabilizing factor of cell shape.

We have come to the conclusion, however, that the current controversy surrounding the tensegrity hypothesis draws attention (28) to what appears to be only a secondary issue: the putative role of internal struts and the merely semantic point of operating definitions. In doing so, it overshadows almost entirely the issue of the central role of the prestress as the key stabilizing factor in cytoskeletal mechanics. This question of mechanism stands regardless of how the prestress might be balanced.

We thank Dr. Yu-Li Wang for teaching us how to make polyacrylamide gel, Dr. Rick Rogers and Jean Lai for confocal microscopy, Z. Liang for assistance, and Dr. Don Ingber for discussion. We also thank Dr. R. Panettieri for supplying HASM cells.

This work was supported by National Heart, Lung, and Blood Institute Grants HL-65371 and HL-33009 and by National Aeronautics and Space Administration Grant NAG5-4839.

REFERENCES

1. **Albrecht-Buehler G.** Role of cortical tension in fibroblast shape and movement. *Cell Motil Cytoskeleton* 7: 54–67, 1987.
2. **An SS and Fredberg JJ.** Cell stiffness: the role of contractile machinery within cultured airway smooth muscle cells (Abstract). *Am J Respir Crit Care Med* 163: A974, 2001.
3. **Babalan BQ, Schwartz US, Riverline D, Goichberg P, Sabanay I, Mahulug D, Safran S, Bershadsky A, Addadi L, and Geiger B.** Force and focal adhesion assembly: a close relationship studied using elastic micropatterned substrates. *Nat Cell Biol* 3: 466–472, 2001.
4. **Brown RA, Talas G, Porter RA, McGrouther DA, and Eastwood M.** Balanced mechanical forces and microtubule contribution to fibroblast contraction. *J Cell Physiol* 169: 439–447, 1996.
5. **Budiansky B and Kimmel E.** Elastic moduli of lungs. *ASME J Appl Mech* 54: 351–358, 1987.
6. **Burridge K, Fath K, Kelly T, Nucholls G, and Turner C.** Focal adhesions: transmembrane junctions between the extracellular matrix and the cytoskeleton. *Annu Rev Cell Biol* 4: 487–525, 1988.
7. **Butler JP, Tolić-Nørrelykke IM, Fabry B, and Fredberg JJ.** Estimating traction fields, moments, and strain energy that cells exert on their surroundings. *Am J Physiol Cell Physiol* 282: C595–C605, 2002.
8. **Calladine CR.** Buckminster Fuller's "tensegrity" structures and Clerk Maxwell's rules for the construction of stiff frames. *Int J Solids Struct* 14: 161–172, 1978.
9. **Chicurel ME, Chen CS, and Ingber DE.** Cellular control lies in the balance of forces. *Curr Opin Cell Biol* 10: 232–239, 1998.
10. **Connelly R and Vack A.** Mathematics and tensegrity. *Am Sci* 86: 142–152, 1998.
11. **Coughlin MF and Stamenović D.** A tensegrity structure with buckling compression elements: application to cell mechanics. *ASME J Appl Mech* 64: 480–486, 1997.
12. **Coughlin MF and Stamenović D.** A tensegrity model of the cytoskeleton in spread and round cells. *ASME J Biomech Eng* 120: 770–777, 1998.
13. **Davies PF.** Flow-mediated endothelial mechanotransduction. *Physiol Rev* 75: 519–560, 1995.
14. **Dembo M and Wang YL.** Stresses at the cell-to-substrate interface during locomotion of fibroblasts. *Biophys J* 76: 2307–2316, 1999.
15. **Discher DE, Boal DH, and Boey SK.** Simulations of the erythrocyte cytoskeleton at large deformation. II. Micropipette aspiration. *Biophys J* 75: 1584–1597, 1998.
16. **Evans E and Yeung A.** Apparent viscosity and cortical tension of blood granulocytes determined by micropipet aspiration. *Biophys J* 56: 151–160, 1989.
17. **Fabry B, Maksym GN, Butler JP, Glogauer M, Navajas D, and Fredberg JJ.** Scaling the microrheology of living cells. *Phys Rev Lett* 87: 148102, 2001.
18. **Fabry B, Maksym GN, Hubmayr RD, Butler JP, and Fredberg JJ.** Implications of heterogeneous bead behavior on cell mechanical properties measured with magnetic twisting cytometry. *J Magnetism Magnetic Mat* 194: 120–125, 1999.
19. **Fabry B, Maksym GN, Shore SA, Moore PE, Panettieri RA, Butler JP, and Fredberg JJ.** Time course and heterogeneity of contractile responses in cultured human airway smooth muscle cells. *J Appl Physiol* 91: 986–994, 2001.
20. **Fredberg JJ, Jones KA, Nathan M, Raboudi S, Prakash YS, Shore SA, Butler JP, and Sieck GC.** Friction in airway smooth muscle: mechanism, latch, and implications in asthma. *J Appl Physiol* 81: 2703–2712, 1996.
21. **Fuller B.** Tensegrity. *Portfolio Artnews Annu* 4: 112–127, 1961.
22. **Fung YC and Liu SQ.** Elementary mechanics of the endothelium of blood vessels. *ASME J Biomech Eng* 115: 1–12, 1993.
23. **Heidemann SR, Kaech S, Buxbaum RE, and Matus A.** Direct observations of the mechanical behaviors of the cytoskeleton in living fibroblasts. *J Cell Biol* 145: 109–122, 1999.
24. **Hiramoto Y.** Mechanical properties of sea urchin eggs. I. Surface force and elastic modulus of the cell membrane. *Exp Cell Res* 56: 201–208, 1963.
25. **Hochmuth RA.** Micropipette aspiration of living cells. *J Biomech* 33: 15–22, 2000.
26. **Hubmayr RD, Shore SA, Fredberg JJ, Planus E, Panettieri RA Jr, Moller W, Heyder J, and Wang N.** Pharmacological activation changes stiffness of cultured human airway smooth muscle cells. *Am J Physiol Cell Physiol* 271: C1660–C1668, 1996.
27. **Ingber DE.** Cellular tensegrity: defining new rules of biological design that govern the cytoskeleton. *J Cell Sci* 104: 613–627, 1993.
28. **Ingber DE, Heidemann SR, Lamoroux P, and Buxbaum RE.** Opposing views on tensegrity as a structural framework for understanding cell mechanics. *J Appl Physiol* 89: 1663–1670, 2000.
29. **Janmey PA.** The cytoskeleton and cell signaling: component, localization, and mechanical coupling. *Physiol Rev* 78: 763–781, 1998.
30. **Jones WR, Ting-Beall HP, Lee GM, Kelly SS, Hochmuth RM, and Guilak F.** Alterations in the Young's modulus and volumetric properties of chondrocytes isolated from normal and osteroarthritic human cartilage. *J Biomech* 32: 119–127, 1999.
31. **Kawai M and Brandt PW.** Sinusoidal analysis: a high resolution method for correlating biochemical reactions with physiologic processes in activated skeletal muscles of rabbit, frog and crayfish. *J Muscle Res Cell Motil* 1: 279–303, 1980.
32. **Laporte JD, Moore PE, Schwartzman I, Panettieri RA, and Shore SA.** p38 MAP kinase regulate IL-1β responses in cultured airway smooth muscle cells. *Am J Physiol Lung Cell Mol Physiol* 279: L932–L941, 2000.
33. **Maksym GN, Fabry B, Butler JP, Navajas D, Laporte JD, and Fredberg JJ.** Mechanical impedance of the cultured human airway smooth muscle cell from 0.05 to 04 Hz. *J Appl Physiol* 89: 1619–1632, 2000.

34. **Mehta D and Gunst SJ.** Actin polymerization stimulated by contractile activation regulates force development in canine tracheal smooth muscle. *J Physiol (Lond)* 519: 829–840, 1999.
35. **Mijailovich SM, Stamenović D, Brown R, Leith DE, and Fredberg JJ.** Dynamic moduli of rabbit lung tissue and pigeon ligamentum propatagiale undergoing uniaxial cyclic loading. *J Appl Physiol* 76: 773–782, 1994.
36. **Moore PE, Laporte JD, Silverman E, Abraham JH, Schwartzman IN, Yandava CP, Drazen JM, Wand MP, Panettieri RA, and Shore SA.** Polymorphisms of the β_2-adrenergic receptor gene and desensitization in human airway smooth muscle. *Am J Respir Crit Care Med* 162: 2117–2124, 2000.
37. **Panettieri RA, Murray RK, DePalo LR, Yadvish RA, and Kotlikoff MI.** A human airway smooth muscle cell line that retains physiological responsiveness. *Am J Physiol Cell Physiol* 256: C329–C335, 1989.
38. **Pelham RJ and Wang YL.** Cell locomotion and focal adhesions are regulated by substrate flexibility. *Proc Natl Acad Sci USA* 94: 13661–13665, 1997.
39. **Pourati J, Maniotis A, Spiegel D, Schaffer JL, Butler JP, Fredberg JJ, Ingber DE, Stamenović D, and Wang N.** Is cytoskeletal tension a major determinant of cell deformability in adherent endothelial cells? *Am J Physiol Cell Physiol* 274: C1283–C1289, 1998.
40. **Pugh A.** *Introduction to Tensegrity*. Berkeley, CA: Univ. of California Press, 1976.
41. **Ricci D, Tedesco M, and Grattarola M.** Mechanical and morphological properties of living 3T6 cells probed via scanning force microscopy. *Microsc Res Tech* 36: 165–171, 1997.
42. **Satcher RL and Dewey CF Jr.** Theoretical estimates of mechanical properties of endothelial cell cytoskeleton. *Biophys J* 71: 109–118, 1996.
43. **Sato M, Theret DP, Wheeler LT, Oshima N, and Nerem RM.** Application of micropipette technique to the measurement of cultured porcine aortic endothelial cell viscoelastic properties. *ASME J Biomech Eng* 112: 263–268, 1990.
44. **Stamenović D and Coughlin MF.** The role of prestress and architecture of the cytoskeleton and deformability of cytoskeletal filaments in mechanics of adherent cells: a quantitative analysis. *J Theor Biol* 201: 63–74, 1999.
45. **Stamenović D and Coughlin MF.** A quantitative model of cellular elasticity based on tensegrity. *ASME J Biomech Eng* 122: 39–43, 2000.
46. **Stamenović D, Fredberg JJ, Wang N, Butler JP, and Ingber DE.** A microstructural approach to cytoskeletal mechanics based on tensegrity. *J Theor Biol* 181: 125–136, 1996.
47. **Stamenović D, Mijailovich SM, Tolić-Nørrelykke IM, Chen J, and Wang N.** Cell prestress. II. Contribution of microtubules. *Am J Physiol Cell Physiol* 282: C617–C624, 2002.
48. **Stamenović D and Wang N.** Invited review: engineering approaches to cytoskeletal mechanics. *J Appl Physiol* 89: 2085–2090, 2000.
49. **Tang D, Mehta D, and Gunst SJ.** Mechanosensitive tyrosine phosphorylation of paxillin and focal adhesion kinase in tracheal smooth muscle. *Am J Physiol Cell Physiol* 276: C250–C258, 1999.
50. **Theret DP, Levesque MJ, Sato M, Nerem RM, and Wheeler LT.** The application of a homogeneous half-space model in the analysis of endothelial cell micropipette measurements. *ASME J Biomech Eng* 110: 190–199, 1988.
51. **Volokh KY and Vilnay O.** New cases of reticulated underconstrained structures. *Int J Solids Struct* 34: 1093–1104, 1997.
52. **Wang N, Butler JP, and Ingber DE.** Mechanotransduction across cell surface and through the cytoskeleton. *Science* 260: 1124–1127, 1993.
53. **Wang N and Ingber DE.** Control of cytoskeletal mechanics by extracellular matrix, cell tension, and mechanical stress. *Biophys J* 66: 2181–2189, 1994.
54. **Wang N and Ingber DE.** Probing transmembrane mechanical coupling and cytomechanics using magnetic twisting cytometry. *Biochem Cell Biol* 73: 327–335, 1995.
55. **Wang N, Naruse K, Stamenović D, Fredberg JJ, Mijailovich SM, Tolić-Nørrelykke IM, Polte T, Mannix R, and Ingber DE.** Mechanical behavior in living cells consistent with the tensegrity model. *Proc Natl Acad Sci USA* 98: 7765–7770, 2001.
56. **Wang N and Stamenović D.** Contribution of intermediate filaments to cell stiffness, stiffening and growth. *Am J Physiol Cell Physiol* 279: C188–C194, 2000.
57. **Wendling S, Planus E, Laurent VM, Barbe L, Mary A, Oddou C, and Isabey D.** Role of cellular tone and microenvironmental conditions on the cytoskeleton stiffness assessed by tensegrity model. *Eur Phys J Appl Physiol* 9: 51–62, 2000.
58. **Yeung A and Evans E.** Cortical shell-liquid model for passive flow of liquid-like spherical cells into micropipets. *Biophys J* 56: 139–149, 1989.
59. **Yoneda M.** Tension at the surface of sea urchin eggs on the basis of "liquid drop" concept. *Adv Biophys* 4: 153–190, 1973.
60. **Zahalak G, McConnaughey WB, and Elson EL.** Determination of cellular mechanical properties by cell poking, with an application to leukocytes. *ASME J Biomech Eng* 112: 283–294, 1990.
61. **Ziemann F, Radler J, and Sackmann E.** Local measurement of viscoelastic moduli of entangled actin networks using an oscillating magnetic bead micro-rheometer. *Biophys J* 66: 2210–2216, 1994.